Chemical Engineering Science 281 (2023) 119163

Contents lists available at ScienceDirect

Chemical Engineering Science

journal homepage: www.elsevier.com/locate/ces

A model for foam fractionation with spatially varying bubble size

Paul Grassia [a,*], Carlos Torres-Ulloa [a,b,c]

[a] Department of Chemical and Process Engineering, University of Strathclyde, James Weir Building, 75 Montrose Street, Glasgow, G1 1XQ, UK
[b] Centro de Investigación, Innovación y Creación (CIIC), Universidad Católica de Temuco, Rudecindo Ortega 03690, Temuco, Chile
[c] Departamento de Ciencias Matemáticas y Físicas, Facultad de Ingeniería, Universidad Católica de Temuco, Rudecindo Ortega 03694, Temuco, Chile

ARTICLE INFO

Keywords:
Foam fractionation
Foam drainage
Liquid fraction in foam
Bubble size
Separation of surface active material
Mathematical modelling

ABSTRACT

A model is developed for a foam fractionation process, supposing that bubble size increases moving up the foam column. Predictions are obtained for liquid flux through the foam column, liquid fraction at the top and enrichment of surface actives within the foamate. Compared to previous models with fixed bubble size, fractionation performance is shown to be improved. A synergy is revealed between the effect of the foam becoming drier (and hence richer in surface actives) as the foam column becomes taller, and the effect of bubble size increasing moving upwards (which makes the foam even drier and hence richer still). A dimensionless parameter m_* quantifies the relative variation in bubble size between top and bottom for a foam column of typical height. Even small m_* values lead to behaviour qualitatively different from a system with no bubble size variation whatsoever, whilst increasing m_* leads to even better fractionation performance.

1. Introduction

Foam fractionation is a promising separation technique (Lemlich, 1968, 1972; Stevenson, 2012, 2014) in many applications involving surface active materials. Such materials adsorb to bubble surfaces. Hence when a foam is created and the resulting foamate is collected (Martin et al., 2010), it is richer in surface actives than the original feed liquid was.

Compared to a conventional separation technique like distillation, fractionation has comparatively low energy requirements. It can also perform even when feed solutions are dilute (King, 1980; Li et al., 2016; Tian et al., 2018). It is moreover a gentle technique that is employed for separating surface active materials that might have poor thermal stability, such as proteins or biomolecules more generally (Brown et al., 1990; de Lucena et al., 1996; Lockwood et al., 1997; Saleh and Hossain, 2001; Du et al., 2002; Crofcheck et al., 2003; Backleh-Sohrt et al., 2005; Gerken et al., 2006; Linke et al., 2007; Shea et al., 2009; Liu et al., 2017). Indeed fractionation has been employed in biotechnology applications (Burghoff, 2012; Díaz De Rienzo et al., 2016; Wu et al., 2020a; Keshavarzi et al., 2022a) and also in wastewater treatment (Mathews et al., 1979; Mukhopadhyay et al., 2010; Kou et al., 2015; Li et al., 2018; Wu et al., 2020b; Buckley et al., 2022).

Improving the design and operation of fractionation systems can be facilitated by having physical models available (Du et al., 2000; Stevenson and Jameson, 2007; Hutzler et al., 2013; Tobin et al., 2014; Keshavarzi et al., 2022b). Unsurprisingly, given that fractionation involves adsorption of surface actives, models must necessarily incorporate a description of the physical chemistry of adsorption. In fact the target materials mentioned earlier for separation (proteins and biomolecules) can exhibit particularly complex adsorption behaviour because they can adsorb in many different states (Fainerman et al., 2003; Miller et al., 2004; Gochev et al., 2013).

Over and above describing adsorption, additional physics is required within models. Injecting air into a liquid to form foam (as happens during fractionation) creates a multiphase system, and hence involves aspects of multiphase flow, which must therefore be incorporated within models also. A typical fractionation column contains a column of foam (hereafter "foam column") towards the top, and a bubbly liquid phase underneath: note the distinction made here between the "fractionation column" and the "foam column", with the latter filling just part of the former. Complex multiphase flow processes occur, as described below, both in the underlying bubbly liquid phase (Sarhan et al., 2017a,b, 2018b) and in the foam itself (Verbist et al., 1996; Weaire et al., 1997; Koehler et al., 1999, 2000).

For instance, air can be introduced at different rates, and the resulting flow velocities within the bubbly liquid phase determine the balance between bubble break up and bubble coalescence events (Sarhan et al., 2017a,b, 2018b). This then determines the bubble size entering the

* Corresponding author.
E-mail address: paul.grassia@strath.ac.uk (P. Grassia).

https://doi.org/10.1016/j.ces.2023.119163
Received 31 May 2023; Received in revised form 2 August 2023; Accepted 5 August 2023
Available online 16 August 2023

foam and ultimately the surface area flux (Sarhan et al., 2018a) within it. It is in fact the foam rather than the bubbly liquid which is the focus of the present work, so the foam is discussed next.

Coalescence can also continue within the foam itself. However the extent of coalescence there can be sensitive to the amount of surface active material present (Keshavarzi et al., 2022b). On the film scale, this then impacts upon transport of surface actives along a foam film, which is itself a complicated process (Yeo et al., 2001; Vitasari et al., 2013; Rajabi and Grassia, 2023). However, in the context of fractionation, what is relevant is that typically having more surface active material present implies better foam stability and hence less coalescence (Keshavarzi et al., 2022b). Remember though that fractionation may often be used for quite dilute systems (King, 1980; Li et al., 2016; Tian et al., 2018) with comparatively little surface active material actually present.

Another parameter that is found to affect the fractionation performance (Stevenson, 2012, 2014) is the foam liquid fraction. The drier the foam, the more enriched the foamate can be (Hutzler et al., 2013; Tobin et al., 2014; Grassia, 2023), because a specified amount of adsorbed surface active that is carried on bubble surfaces is then accompanied by very little bulk liquid.

To summarise then, knowing how liquid is distributed within and transported through the foam phase (Neethling et al., 2000) is therefore important for modelling fractionation performance. It turns out that such transport is governed by foam drainage theory, involving a balance between liquid convection by air, gravity-driven liquid drainage and capillary suction effects (Verbist et al., 1996; Weaire et al., 1997; Koehler et al., 1999, 2000; Grassia et al., 2001; Lorenceau et al., 2009). Foam drainage is typically an unsteady state process (Verbist et al., 1996; Cox et al., 2000; Neethling et al., 2005; Grassia et al., 2006; Brito-Parada et al., 2013), and a model for foam fractionation can be set up (Keshavarzi et al., 2022b) to capture that unsteady behaviour.

Nevertheless even simplified drainage theories (Grassia et al., 2001) (assuming e.g. liquid fluxes that are spatially uniform and also temporally steady (Hutzler et al., 2013; Tobin et al., 2014) or quasi-steady (Grassia, 2023)) can make useful predictions about fractionation performance: indeed quasi-steady state drainage behaviour tends to set up on a time scale that is short compared to the duration of a typical fractionation process (Grassia, 2023). It can then be shown for instance (Hutzler et al., 2013; Tobin et al., 2014; Grassia, 2023) that making the foam column taller also makes it drier and hence enriched in surface actives, whilst decreasing air flow velocity has the same effect.

The effect of increasing bubble size entering the foam is less straightforward. On the one hand, larger bubbles have lower specific surface area (Pitois et al., 2009) and hence have less adsorbed surface active per total foam volume. On the other hand, larger bubbles drain more readily (Hilgenfeldt et al., 2001) and as a result have lower liquid content per total foam volume. In enrichment terms, it turns out that the latter effect outweighs the former (Grassia, 2023).

There was however one significant element missing from the simple models discussed above. Even though the effect of having various different bubble sizes was considered (Grassia, 2023), the bubble size was assumed to be spatially uniform throughout the foam column. In fact it has been found (Keshavarzi et al., 2022b; Tong et al., 2011) that bubble size actually grows moving up through a foam column, with the change in bubble size being more significant when the concentration of surface actives is low (Keshavarzi et al., 2022b). There is potential now for the spatially varying bubble size to impact fractionation performance, and thus likewise for foam stability to impact performance (Neethling and Brito-Parada, 2018).

The aim of the current study therefore is to incorporate spatially varying bubble size as considered by Keshavarzi et al. (2022b) into the comparatively simple foam drainage models considered by Hutzler et al. (2013); Tobin et al. (2014); Grassia (2023), and consequently to make novel predictions about fractionation performance. As we will see this leads, not just to quantitative differences in predicted performance, but qualitative differences as well. Moreover, as will be explained later, a synergy will be shown to arise between the effects of increasing foam column height and increasing bubble size.

The rest of this paper is organised as follows. Section 2 presents the models to be employed. Section 3 analyses the models, and then section 4 presents results. Finally section 5 offers conclusions. Additional information about the models is also provided in supplementary material.

2. Foam fractionation model

The simple model for foam fractionation used here involves three elements. The first element (section 2.1) is a description of liquid flux through the foam column, and the associated variation in liquid fraction over the height of the foam column. The second element (section 2.2) is the variation in bubble size. The third element (section 2.3) is the enrichment of the foamate, or equivalently the effective concentration of surface actives in the foamate. Here, as in Grassia (2023), the model will be presented in dimensionless form. Dimensional analogues are presented in sections S1–S2 in supplementary material. To give a sense of scale in what follows, we also indicate in due course what each dimensionless unit typically represents in actual physical units.

2.1. Model for liquid flux through and liquid fraction within the foam

We follow the same model for liquid flux through the foam column Q_{thru} as was used by Grassia (2023), just with a minor modification to account for variation in bubble size. Models developed by Hutzler et al. (2013); Tobin et al. (2014) are similar, but the notation used in the model of Grassia (2023) lends itself more readily to considering variation in bubble size. The model can be written

$$Q_{\text{thru}} = V_{\text{air}}\phi - R^2\phi^2 - R^{-1}\phi^{1/2}\partial(\phi R^2)/\partial Y. \tag{1}$$

The terms on the right hand side represent respectively convection of liquid by the air, gravity drainage and the effect of capillary suction. Here ϕ is foam liquid fraction. Also V_{air} is dimensionless air velocity (a typical value according to Grassia (2023) is 0.00195; see Table 1). Note that (see Grassia (2023) and also section S1 in supplementary material) one unit of dimensionless velocity corresponds to a physical velocity of around 0.056 m s^{-1}. As section S1 explains in detail, this velocity unit is essentially σ/μ (σ being surface tension and μ being liquid viscosity), with some additional prefactors associated with foam geometry. Section S1 explains that changing from one fractionation system to another has barely any impact on the value of this characteristic unit of velocity.

In addition R is dimensionless bubble radius (discussed further in section 2.2) and Y is dimensionless vertical coordinate (measured upwards). The reason for using partial derivative notation with respect to Y is explained in section S1. Equation (1) applies over the domain $0 \le Y \le L$ where L denotes the dimensionless foam column height. Here one unit of dimensionless length (see Grassia (2023) and also section S1) corresponds to a physical length around 1.3×10^{-3} m. Section S1 explains that this length unit is essentially $(\sigma/(\rho g))^{1/2}$ (with σ being surface tension, ρ being density of liquid in the foam and g being gravity acceleration), but with some prefactors associated with foam geometry. Again section S1 explains that changing from one fractionation system to another has barely any impact on the value of this characteristic unit of length.

Note also in equation (1) the derivative that is acting on ϕR^2 rather than just on ϕ. Here ϕR^2 is in effect a dimensionless measure of the Plateau border cross-sectional area. Indeed the capillary suction pressure associated with Plateau borders (Weaire and Hutzler, 1999) is a function of the cross-sectional area rather than solely a function of liquid fraction. If R is spatially uniform, then the model of Grassia (2023) is recovered. On the other hand, if R varies spatially even at fixed ϕ, then the capillary pressure also varies, and equation (1) accounts for that.

Table 1
Dimensionless parameter values held fixed here. Other parameter values appearing in the model such as ϕ_{top}, R_{top}, m_* and L will be selected with various different values.

Parameter	Symbol	Value
Dimensionless air velocity	V_{air}	0.00195
Dimensionless bubble radius at bottom of foam	R_0	0.25
Liquid fraction at bottom of foam	ϕ_{bot}	0.36
Typical/base case dimensionless foam column height	L_{base}	40
Dimensionless surface active adsorption parameter	Γ_{0*}	0.025

Another minor point we mention (Hutzler et al., 2013; Tobin et al., 2014; Grassia, 2023) is that equation (1) formally assumes a dry limit $\phi \ll 1$. What this means is that liquid volume fraction ϕ might vary in relative terms by orders or magnitude across the height of the foam column, whereas the relative variation of air volume fraction $1-\phi$ is less. Under these circumstances, air flux and air velocity are essentially the same, and thus air velocity V_{air} can be treated as spatially uniform. The forms of the gravity drainage and capillary suction terms within equation (1) also assume a dry limit. These terms would need to take more complicated forms in wetter foams (Lorenceau et al., 2009; Höhler et al., 2021).

Equation (1) needs to be solved with boundary conditions. At the bottom, we impose a condition $\phi = \phi_{bot}$ where we set $\phi_{bot} = 0.36$ (Grassia, 2023; Cantat et al., 2013). This boundary condition is used (Grassia, 2023) despite it extrapolating equation (1) beyond the dry limit. Typically however foam columns are tall enough so as to be dry over most of their height, away from the bottom.

At the top we impose a "no slip" condition that the velocity of liquid and air are the same. In other words $Q_{thru} = \phi_{top} V_{air}$ or equivalently $\phi_{top} = Q_{thru}/V_{air}$ where ϕ_{top} is the liquid fraction at the top. This supposes (see Grassia (2023) for more explanation) that (in line with experimental observations on a particular fractionation system by Keshavarzi et al. (2022b)) there is no significant bursting of foam films right at the top: this is what then requires liquid and air to have the same velocity there. Analogous boundary conditions also apply in the gravity thickening of suspensions (for detail, see Grassia (2023) and references therein, e.g. Fitch (1966); Usher and Scales (2005)). Returning to consider the case of foam fractionation, internal coalescence of bubbles (leading to spatial variation of bubble size) is still permitted (Keshavarzi et al., 2022b), and will be discussed in section 2.2.

What is apparent is that two boundary conditions have been imposed here, but equation (1) is only a first order differential equation. This implies that there must be a relationship between the foam column height L and the liquid fraction at the top ϕ_{top}. Establishing this relationship is an essential part of solving for the fractionation performance. The relationship in question is sensitive to spatial variation in the bubble radius, so this is considered next.

2.2. Model for changes in bubble radius

The novel aspect taken into account in the model employed here is spatial variation of bubble size resulting from bubble-bubble coalescence inside the foam. The work of Keshavarzi et al. (2022b) considered bubble size to vary linearly with vertical coordinate. We adopt the same approach here. Specifically we assume

$$R = R_0(1 + m_* Y / L_{base}). \tag{2}$$

Here R_0 is the bubble radius entering the bottom of the foam column (a typical value according to Grassia (2023) is 0.25 dimensionless units; see Table 1). In addition L_{base} is a typical base case height of the foam column during a fractionation experiment (a suitable value according to Grassia (2023) is 40 dimensionless units; see Table 1): note that L_{base} is merely a typical value, and the actual foam column height L might well differ from it. Recall also (see Grassia (2023) and section S1) that one unit of dimensionless length corresponds to a physical length around 1.3×10^{-3} m.

Finally m_* is a parameter that measures the stability of the bubbles against coalescence. The value of m_* depends on the amount of surface active agent present: higher concentration of surface actives implies smaller m_*, whereas lower concentration of surface actives implies larger m_*. Of course the concentration of surface actives must never be so low that the foam collapses entirely before it manages flow out of the fractionation system (Tobin et al., 2014): in order to enrich the surface active at all it is essential to collect at least some foamate.

Experimental data suggest that m_* might be in the domain 0.5 to 2 (Keshavarzi et al., 2022b), although simulations have considered values of m_* covering a domain 0.2 to 10 (Keshavarzi et al., 2022b). Remember here that larger values of m_* would typically correspond physically to smaller surfactant concentrations, whereas smaller values of m_* would correspond to larger surfactant concentrations. In principle, the value of m_* might also be dependent upon air flow rate (dimensionless parameter V_{air}) and upon bubble size (dimensionless parameter R_0). This could then indicate m_* being sensitive to the profile of liquid fraction (ϕ vs Y, which itself depends on V_{air} and R_0 according to equation (1)). Intuitively a wetter foam (corresponding to higher V_{air} and/or smaller R_0) might be less susceptible to bubble-bubble coalescence than a drier foam would be. However we do not consider such aspects because they were not considered by Keshavarzi et al. (2022b) (only the effect upon m_* of changing surfactant concentration was explored, as already mentioned).

Clearly $m_* = 1$ corresponds to bubble size doubling between $Y = 0$ and $Y = L_{base}$. It is permitted to select foam columns of height very different from L_{base}. If we choose a shorter (taller) initial column, there is less (more) variation in bubble size R seen than in the base case.

Likewise, over time, the foam column height grows as liquid is removed from beneath the foam, and so we also see more variation in bubble size. However (unlike the work of Keshavarzi et al. (2022b); Grassia (2023)) time variation is not considered here. We look instead just at instantaneous fractionation performance as Hutzler et al. (2013); Tobin et al. (2014) did. A further comment is that the model as written only depends on the ratio m_*/L_{base} and not on the values of m_* and L_{base} separately. Even so, it is convenient to define both parameters, because it means that, when L_{base} is set to a specified value (Grassia, 2023) (as will be done here; see Table 1), the value m_* then gives a more direct measure of relative variation in bubble size for a foam of typical height.

2.3. Surfactant flux and effective concentration

In addition to a model for liquid transport we also need a model for transport of surface actives and ultimately enrichment of surface actives. How surface actives behave in a foam, and in particular how they distribute between being dissolved within liquid and being adsorbed on foam film surfaces is a complicated topic (Keshavarzi et al., 2022b), particularly when (Fainerman et al., 2003; Gochev et al., 2013) the surface active material happens to be a bulky molecule like a protein (often targeted in fractionation applications), as opposed to being just a simple surfactant. Here following Grassia (2023) we adopt a highly simplified model: this supposes that if a typical value of surface active concentration within bulk liquid in the foam is given, then a typical value of the amount of adsorbed surface active is also known. Parameter values within the model are informed by Keshavarzi et al. (2022b). Details of this are described in section S2 in supplementary material but we summarise the key points below.

The dimensionless effective concentration C_{eff} is a measure of how enriched the foamate is relative to the feed. It satisfies

$$C_{eff} = 1 + \Gamma_{0*}/(R_{top}\phi_{top}). \tag{3}$$

Here R_{top} is dimensionless bubble size at the top and ϕ_{top} is liquid fraction at the top. Also Γ_{0*} (see section S2) is a dimensionless parameter associated with adsorption of surface actives. Physically Γ_{0*}

is a ratio between a typical surface concentration and a typical bulk concentration normalised by a length $(\sigma/(\rho g))^{1/2}$, with some geometrical prefactors (see section S2). The value of Γ_{0*} is sensitive to foam physical chemistry, but not to parameters like air velocity V_{air}, foam column height L or bubble size R_0. A typical value is $\Gamma_{0*} \approx 0.025$ (see Grassia (2023) and also Table 1) and we use that value throughout. To give a sense of scale, we mention that one unit of dimensionless concentration in equation (3) might correspond to an actual concentration (Grassia, 2023; Keshavarzi et al., 2022b) of surface active on the order of 0.1 kg m^{-3} within liquid.

What we anticipate is that increasing foam column height causes C_{eff} to grow, and hence the foam to become enriched in surface actives. This is anticipated to happen for two reasons. Firstly taller columns tend to be drier (Grassia, 2023) (ϕ_{top} is smaller). Secondly taller columns have larger bubbles, and increasing bubble size should cause ϕ_{top} to fall even more significantly still. This then is the basis for the expected synergy between foam column height and bubble size acting to enrich the foam. Results are discussed in section 4, but before doing that, in section 3, we consider how the model behaves in a more qualitative fashion.

3. Analysis of model behaviour

The model to be solved here is defined by equations (1)–(3) along with the boundary conditions already described in section 2.1. The model is easy to solve numerically (see details in section S3 in supplementary material). Before considering numerical model solutions however, one of the ways of analysing the system behaviour (Grassia, 2023) is graphically by sketching, as a function of liquid fraction ϕ, various contributions to the liquid flux denoted Q. It must be remembered however that these contributions necessarily sum to a spatially uniform value Q_{thru} with liquid fraction at the top then given by $\phi_{\text{top}} = Q_{\text{thru}}/V_{\text{air}}$. Note that if we set a target ϕ_{top} that then determines what the foam column height L must be to achieve that particular ϕ_{top} value. For the foamate to become enriched, we need ϕ_{top} to be significantly smaller than ϕ_{bot}, i.e. the foam should become dry at the top. In what follows we analyse a case that is indeed "relatively dry" at the top (in a sense to be made more precise shortly), and then a case which is much drier still.

3.1. Case of a relatively dry foam at the top

What we show in the present section is as follows. If there is no spatial variation in bubble size, provided (Hutzler et al., 2013; Tobin et al., 2014; Grassia, 2023) the foam is selected to be relatively dry at the top (in a sense to be specified shortly), then the foam column must become very tall (as will also be explained shortly). On the other hand, if there is spatial variation in bubble size as is the case in the present work, then for the same liquid fraction at the top, the foam column does not need to be nearly as tall.

All this can be explained with reference to Fig. 1. In this figure, the sloping line represents $V_{\text{air}}\phi$, the liquid flux convected along with the air flow. Meanwhile the curve (an inverted parabola) represents $V_{\text{air}}\phi - R^2\phi^2$, the liquid flux convected by the air and by gravity drainage taken together. The horizontal line Q_{thru} represents the actual liquid flux carried through the foam, which is spatially uniform. Where the sloping line and the horizontal line intersect defines the liquid fraction at the top of the foam ϕ_{top}, where as mentioned $\phi_{\text{top}} = Q_{\text{thru}}/V_{\text{air}}$. The liquid fraction at the bottom of the foam ϕ_{bot} is typically much larger (shown here by a break in the curve).

Meanwhile the difference between the horizontal line and the inverted parabola represents the capillary suction term, which is given by $-R^{-1}\phi^{1/2}\partial(\phi R^2)/\partial Y$. Suppose now that (as drawn in Fig. 1 for the uppermost inverted parabola) this difference is small, i.e. the peak value Q_{peak} on the inverted parabola is only slightly less than $Q_{\text{thru}} = V_{\text{air}}\phi_{\text{top}}$: this then is what we mean by the system being relatively dry at the top. Given $\partial(\phi R^2)/\partial Y$ is now small (at least for ϕ values close to ϕ_{peak}, which corresponds to the peak on the inverted parabola), if the spatial variation of R is also neglected, then $\partial\phi/\partial Y$ is necessarily small (again for ϕ values close to ϕ_{peak}). We then need a large foam column height for ϕ to evolve from ϕ_{bot} to ϕ_{top}. Indeed much of the height of the foam column is associated with ϕ values around ϕ_{peak}: as already alluded to, the value of ϕ changes only very slowly with Y there.

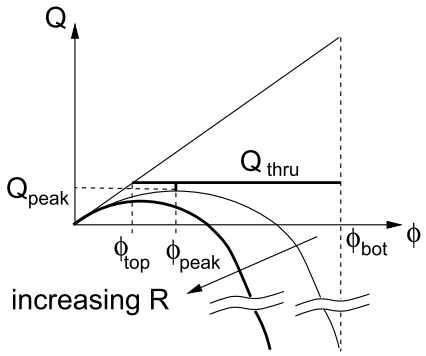

Fig. 1. Various contributions to the liquid flux Q in a foam column depending on the liquid fraction ϕ. The sloping line represents $V_{\text{air}}\phi$, the contribution from convection by air. The inverted parabola represents $V_{\text{air}}\phi - R^2\phi^2$, the combined contribution from air convection and gravity drainage taken together for a specified value of R. This admits a peak value Q_{peak} at a liquid fraction ϕ_{peak}. However the shape of the inverted parabola changes as R changes, so strictly speaking the values of Q_{peak} and ϕ_{peak} should change away from their original values (corresponding to an original bubble size R_0) which are the values marked here. The horizontal line represents the total liquid flux Q_{thru} delivered through the foam column. The difference between the horizontal line and the inverted parabola represents the effect of capillary suction, which is active when ϕ (or more generally ϕR^2) changes spatially: ϕ varies from ϕ_{bot} to ϕ_{top}, with ϕ_{top} corresponding here to the intersection between the sloping line and the horizontal line. As R increases, the inverted parabola shifts downwards, so the difference between the horizontal line and the inverted parabola increases.

Note also that there is a difference in behaviour between a foam which has liquid flux Q_{thru} greater than the peak Q_{peak} on the inverted parabola and a foam which has liquid flux less than the peak on the inverted parabola: this is explained in detail in Grassia (2023). In the former case (which is what we consider here) capillary suction is always relevant: as a result the foam has finite height, and also a boundary condition of no slip between liquid and air (as observed by Keshavarzi et al. (2022b)) can be imposed. In the special case when the liquid flux is just slightly above the peak on the inverted parabola, the foam is finite height but tall (Hutzler et al., 2013; Tobin et al., 2014), and we say the foam is relatively dry at the top. On the other hand, when the liquid flux Q_{thru} is less than the peak on the inverted parabola (not the case we consider here, but a case considered by Grassia et al. (2001); Grassia (2023)), the foam can in principle become arbitrarily tall. High enough up in the foam, capillary suction then eventually becomes unimportant, and the no slip boundary condition cannot then be met.

The situations discussed above, concern spatially uniform values of R. The case of spatially varying R is different however, because R itself grows as ϕ evolves. This affects the shape of the inverted parabola. In the figure, it is the uppermost inverted parabola which now corresponds to $V_{\text{air}}\phi - R_0^2\phi^2$ where (as already mentioned) R_0 is the bubble size entering the foam column at the bottom.

There is however now a family of inverted parabolae, one parabola for each R. The inverted parabola that is drawn lower down in Fig. 1 corresponds to $V_{\text{air}}\phi - R^2\phi^2$ with a larger R value, remembering that R increases here as Y increases. In effect once ϕ has evolved from ϕ_{bot} to the original ϕ_{peak} say, the liquid flux delivered by air convection and gravity drainage combined has shifted from the upper inverted parabola to an inverted parabola that is lower down. In Fig. 1, this is now quite some distance below the horizontal line Q_{thru}. As a result, the capillary term need no longer be small, and hence there is no longer a require-

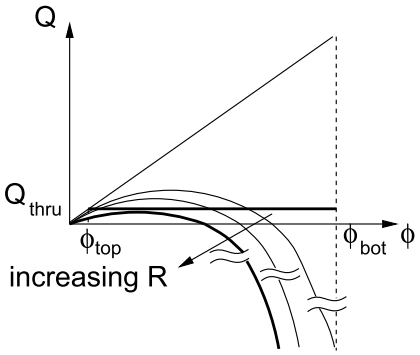

Fig. 2. Various contributions Q to the liquid flux through a foam. In particular the inverted parabola $V_{air}\phi - R^2\phi^2$ represents the combined effect of air convection and gravity drainage. The horizontal line represents the total liquid flux through the system Q_{thru} which is now set at a value below the peak on the inverted parabola. The intersection between the inverted parabola and horizontal line indicates a state with essentially no capillary suction contribution to liquid flux. The value of ϕ at this intersection only changes as the value of R changes, which in turn changes the shape of the inverted parabola. For large enough R, the entire inverted parabola lies below the horizontal line, and capillary terms become relevant again. Liquid fraction ϕ varies from ϕ_{bot} to ϕ_{top}.

ment to have slow spatial changes with Y. In other words there is no longer a requirement for the foam column to become extremely tall for ϕ to vary from ϕ_{bot} all the way to ϕ_{top}.

3.2. Case of a very dry foam at the top

In the previous figure (Fig. 1) we considered a Q_{thru} value slightly greater than Q_{peak} (the peak on the inverted parabola or, more precisely, slightly greater than the peak on the inverted parabola with $R = R_0$). Values of Q_{thru} smaller than this were not considered. Provided R varies spatially, there is however now a mechanism to have Q_{thru} even smaller than the aforementioned Q_{peak}. This then is what is termed a very dry foam.

First consider (see Fig. 2) the issue with selecting Q_{thru} below the peak of the inverted parabola but for spatially uniform R. At the given Q_{thru} (horizontal line) the value of ϕ evolves from ϕ_{bot} to a ϕ value at an intersection point between the horizontal line and the inverted parabola (specifically the ϕ value at the larger of two intersection points: see section S4 in supplementary material for details).

The value of ϕ cannot evolve any further than that, even if the foam column becomes very tall (Grassia, 2023; Grassia et al., 2001). Hence a boundary condition $\phi_{top} = Q_{thru}/V_{air}$ at the intersection between the horizontal line and the sloping line in Fig. 2, cannot be met, at least when R is spatially uniform.

In the case with even slowly spatially varying R, the situation is different. The value of ϕ still becomes held up (i.e. no longer changes much with Y) in the neighbourhood of the intersection between the horizontal line and the inverted parabola. However the inverted parabola itself now changes as R changes, hence as Fig. 2 shows, the ϕ value at the intersection likewise changes (as already mentioned, the resulting formula for ϕ is given in section S4 in supplementary material). For each R value, we can also identify using equation (2), the Y value needed to attain that particular R. A predicted relationship between ϕ and Y then follows, which is accurate provided R is slowly spatially varying, i.e. provided the parameter m_* is small (again section S4 provides details).

There will be a certain value of R (or equivalently a certain Y value) at which, in Fig. 2, the entirety of the inverted parabola falls below the horizontal line. The value of ϕ is no longer held up at the inverted parabola, and so is free now to evolve all the way down to ϕ_{top}.

To summarise, provided bubble size varies only slowly with R, three regions are expected in the ϕ versus Y profile. In one region (lowest down in Y), ϕ changes from ϕ_{bot} to a ϕ value lying on an inverted

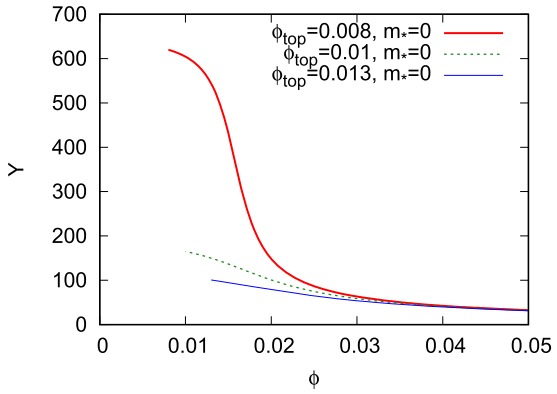

Fig. 3. Liquid fraction profiles ϕ versus coordinate Y. These data correspond to a fixed bubble size (hence $m_* = 0$), and also various values of ϕ_{top} (and hence various values of $Q_{thru} = V_{air}\phi_{top}$). Other parameters are as per Table 1.

parabola. In the second region (intermediate values of Y, but potentially covering a very significant domain of Y values), ϕ evolves only as the inverted parabola itself evolves. In the third region (highest up in Y), ϕ evolves away from the inverted parabola to a value ϕ_{top}.

We emphasise that the above approximation involves an assumption of small m_* values (i.e. slowly spatially varying bubble size). Different sets of approximations apply in the limit of larger m_* values: see sections S5–S6 in supplementary material for details. These latter approximations rely on the observation made earlier that ϕR^2 is a dimensionless measure of the Plateau border cross-sectional area. This turns out to be a convenient quantity to analyse, because to an extent, rapid spatial decay in ϕ with increasing height is compensated by rapid spatial increase in bubble size R. As sections S5–S6 explain, it is then possible to identify which terms in the governing equations are the dominant ones, and approximate accordingly.

4. Results

This results section presents the predictions of the model used here. It starts off by considering how liquid fraction varies with position within a given foam column (section 4.1). It then moves on to look more globally at how foam column height affects liquid fraction at the top (section 4.2), bubble size at the top (section 4.3), and effective surface active concentration in the foamate (section 4.4).

4.1. Profiles of liquid fraction across the foam

Profiles of ϕ versus Y for various ϕ_{top} values are shown in Fig. 3. These data are for a fixed bubble size (i.e. $m_* = 0$), so correspond to the case already studied in Grassia (2023). However they are included here so as to be able to contrast with variable bubble size cases later on. The main observation is that as ϕ_{top} falls, and hence $Q_{thru} = V_{air}\phi_{top}$ likewise falls, the foam column becomes taller. In fact we know (see also Fig. 1) that Q_{thru} approaches a certain limiting value Q_{peak} as the foam column becomes very tall indeed. The smallest permitted ϕ_{top} (i.e. lower bound for ϕ_{top}) is known (Grassia, 2023) to be $V_{air}/(4R^2)$ with $R = R_0$ when $m_* = 0$. For the particular parameters selected here (see Table 1), this leads to a value just slightly below 0.008.

Note moreover that the ϕ domain in Fig. 3 (and some later figures also) is only plotted for $\phi \leq 0.05$, although in principle ϕ can extend all the way up to $\phi_{bot} = 0.36$. For ϕ greater than about 0.05 though (i.e. near the bottom of the foam column), the various different profiles with different Q_{thru} all collapse onto the same curve. This is in line with predictions of Grassia (2023), and follows in fact from equation (1). Given that V_{air} is typically a small parameter (much smaller than R^2, see e.g. Table 1), then provided ϕ is significantly larger than order V_{air}/R^2, the dominant balance in that equation is between gravity drainage downwards and capillary suction upwards (Grassia, 2023).

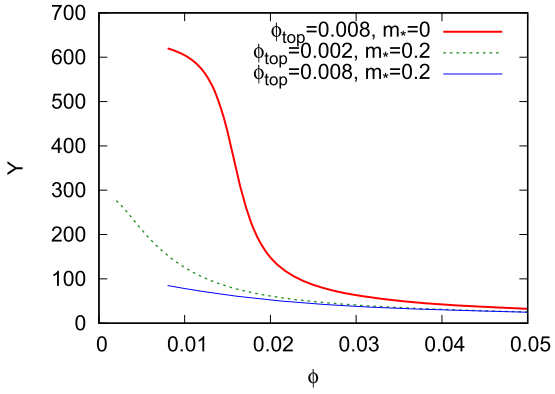

Fig. 4. Liquid fraction profiles comparing cases with no variation in bubble size $m_* = 0$ and with some variation in bubble size $m_* = 0.2$. Various ϕ_{top} values are considered.

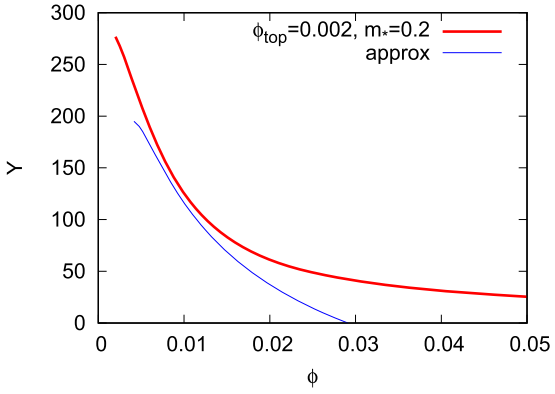

Fig. 5. Profile of ϕ versus Y for $\phi_{\text{top}} = 0.002$ and $m_* = 0.2$. An approximate profile is also shown assuming that solutions for ϕ lie on an inverted parabola in Q versus ϕ space (see section S4), but the shape of the inverted parabola evolves as bubble size R varies with Y.

A so called equilibrium profile then results (see also equation (S15) in the supplementary material). In effect, for the parameter values selected here, there is no need to examine profiles closely for ϕ values greater than about 0.05 as data tend to collapse together as already mentioned. Now we move on to consider cases with nonzero m_*.

In Fig. 4 some cases with a small but nonzero m_* are shown, specifically $m_* = 0.2$. Again we see that reducing ϕ_{top} (hence reducing Q_{thru}) causes the foam column height to increase. More importantly though we can now attain ϕ_{top} values much smaller than would be permitted with $m_* = 0$ and still have a less tall foam column: a profile with $m_* = 0$ is also shown in Fig. 4 for contrast.

In section 3.2 we argued that when Q_{thru} and m_* are small parameters, the profile of ϕ versus Y can be divided into three regions: a lowermost region, an intermediate region (for which an approximate formula for the profile should be available) and an uppermost region. This scenario is verified in Fig. 5. We present the actual ϕ versus Y profile, and the approximate profile (for details of the approximate profile see section S4). As expected, the actual ϕ versus Y profile approaches the approximate one, stays close to it over just part of the spatial domain (specifically for intermediate Y values), but then departs again.

Although Fig. 5 considers just one particular nonzero m_* value, it is possible to argue that the height of the region of intermediate Y values should scale inversely with m_*. This follows because the height of this region is governed (as section 3.2 explains) by the entirety of the inverted parabola $V_{\text{air}}\phi - R^2\phi^2$ becoming smaller than Q_{thru}, whereas to effect a specified change in the function $V_{\text{air}}\phi - R^2\phi^2$, it is necessary to change R by a specified target amount. According to equation (2), this then requires Y to scale inversely with m_*. Equations (S11)–(S12)

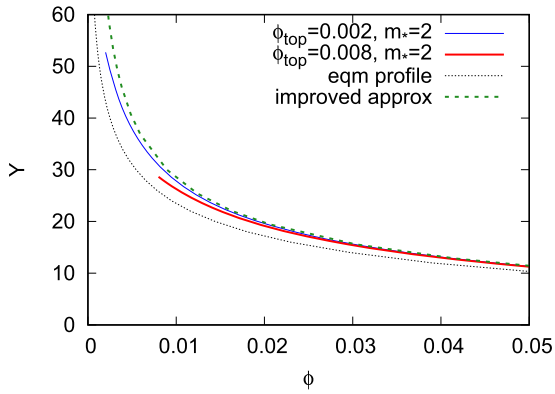

Fig. 6. Profiles of liquid fraction ϕ versus Y for $m_* = 2$ and various ϕ_{top}. Approximations, namely an equilibrium profile and an improvement upon it (discussed in detail in the supplementary material; see section S5), are also shown.

in the supplementary material corroborate this. We have not however presented data with other m_* values within Fig. 5 because reducing m_* would take us outside the domain of m_* contemplated by Keshavarzi et al. (2022b), whereas increasing m_* would reduce the quality of the fit: we are dealing specifically with a small m_* approximation here.

The data we have examined to date were obtained for a small m_* value (bubble size changing only slowly with position). It is also of interest to consider the behaviour with much larger m_* (bubble size changing more rapidly with position). In Fig. 6 we show profiles of ϕ versus Y for $m_* = 2$. Two different values of ϕ_{top} are considered. The profiles with different ϕ_{top} are actually almost the same over much of the domain (remember the domain extends all the way to $\phi_{\text{bot}} = 0.36$, although we have not plotted all of it here). There is however some sensitivity to ϕ_{top} close to the top. It is clear moreover that through having large m_*, very dry foams (low ϕ_{top}) can now be obtained even over comparatively modest heights (contrast Fig. 6 with Fig. 3 through Fig. 5).

Some approximations (see section S5 for details) are available for the shape of the profile: these are plotted also in Fig. 6. The first approximation follows from the observation, already alluded to earlier, that near the bottom of any foam column (or equivalently over the entirety of the foam column in the case of a column that is not too dry at the top (Grassia, 2023)), the dominant balance is between gravity drainage downwards and capillary suction upwards. As mentioned, a so called equilibrium profile then results. This relies (Grassia, 2023), as alluded to earlier, upon ϕ remaining significantly larger than V_{air}/R^2, or equivalently upon V_{air}/R^2 remaining significantly smaller than ϕ. Note also that if R increases moving up the foam column (as is the case here), then it is more likely that V_{air}/R^2 will remain small.

An improved approximation can be obtained by retaining the effect of convection by air within the profile: this is also plotted. Details of what this improved approximation involves can be found in section S5. This now includes regions of the profile in which ϕ need not necessarily be much larger than V_{air}/R^2, although regions right near the top where R can become very large indeed (with ϕ and ϕ_{top} values then being very small) remain excluded. Additional discussion of the data plotted in Fig. 6 can be found in section S7 in supplementary material.

4.2. Foam liquid fraction at the top

Thus far we have presented results in the form of ϕ versus Y profiles for various ϕ_{top} and m_* values. Now we turn to consider results more globally by plotting liquid fraction at the top ϕ_{top} versus the entire foam column height L for various m_*. Data are presented in Fig. 7.

As can be seen in Fig. 7, making the foam column taller clearly also makes it drier (i.e. increasing L, reduces ϕ_{top}). However making bubbles larger is also known in itself to make the foam drier as Grassia

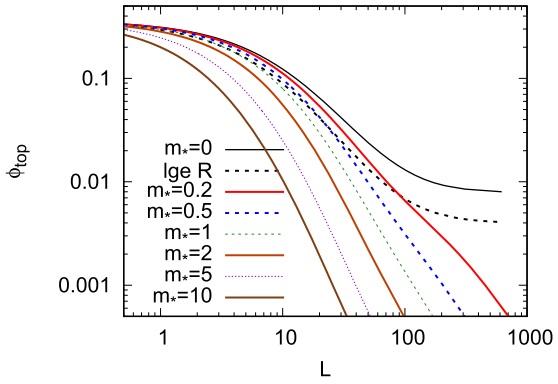

Fig. 7. Liquid volume fraction at the top of the foam column ϕ_{top} versus foam column height L. Various m_* values are considered. The curve labelled "lge R" are data for $m_* = 0$ but with a larger bubble radius (increased by a factor 1.4).

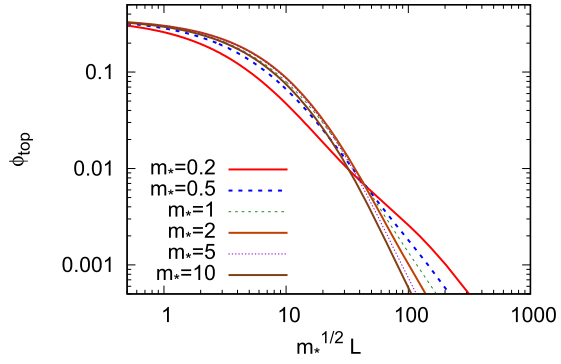

Fig. 8. Values of ϕ_{top} versus $m_*^{1/2}L$ for various m_*.

(2023) showed. Hence in a scenario in which foam column height and foam bubble size are coupled (i.e. for nonzero m_* as we have here), a synergy can emerge: making the foam column taller also makes the bubble size larger, and the combined effect then makes the foam much drier than before. Moreover the stronger the coupling between foam column height and bubble size (i.e. the larger the value of m_*), the drier the foam can become (i.e. ϕ_{top} reduces further for large m_*).

A final observation here is the qualitative difference between the $m_* = 0$ case and the cases with $m_* \neq 0$. When $m_* = 0$ there is a finite lower bound for ϕ_{top} even in cases for which L becomes arbitrarily large. Keeping $m_* = 0$, but increasing the bubble size (by a factor of 1.4, a case also considered by Grassia (2023); in Fig. 7 see the curve labelled "lge R") reduces the value of this lower bound, but a bound remains present. In the case of nonzero m_* however, there is no such lower bound: making the foam column taller also makes the bubbles larger, which helps with reducing ϕ_{top}.

It is clear that increasing m_* pushes ϕ_{top} versus L curves to the left in Fig. 7. We can compensate for this by replotting against $m_*^{1/2}L$. As Fig. 8 shows, this collapses together the data, particularly the data at large m_*. Data for smaller m_* however do not collapse quite so well: they tend to be too far to the left for larger ϕ_{top} and too far to the right for smaller ϕ_{top}. The collapse at large m_* is however in line with predictions from various approximate formulae in the large m_* limit: see section S6 in supplementary material.

Recall that (see e.g. Fig. 6) it was possible to generate various approximate profiles for ϕ versus Y. These same approximations can also be used to generate approximate formulae for ϕ_{top} versus L. The formulae involve either an equilibrium gravity-capillarity balance, or else an improvement upon that taking account of liquid being convected by air (see details in section S5). These approximations (dotted lines) are plotted in Fig. 9 along with the original data (solid lines). Various

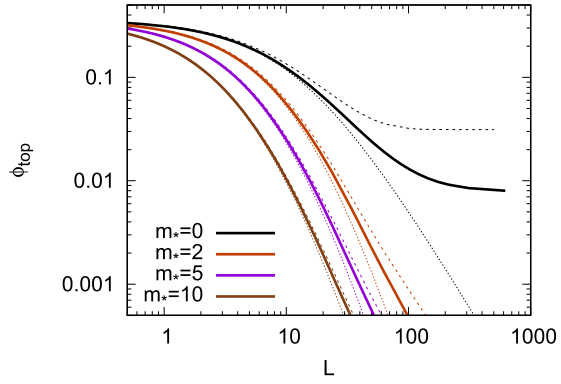

Fig. 9. Values of ϕ_{top} versus L and for various m_*. Also shown (bracketing the actual values) are approximations to ϕ_{top} versus L for each m_*.

m_* values are shown, and in each case the approximations bracket the original data.

Clearly at any given m_*, the approximations perform best when L is small (i.e. when ϕ_{top} is comparatively large), but less well when L increases (i.e. when ϕ_{top} is smaller). That said when m_* is large, the approximate formulae remain valid down to rather smaller ϕ_{top}. In fact the approximate analysis in section S5, is more reliable when ϕ_{top} remains somewhat larger than V_{air}/R^2. This is however relatively easy to achieve when m_* is large because R increases and hence V_{air}/R^2 decreases.

4.3. Bubble size at the top

Thus far we have considered the effect of foam column height L on liquid fraction at the top ϕ_{top}. However ϕ_{top} is not the only physical parameter of interest here. It is also of interest to ask how bubble size at the top R_{top} and effective surface active concentration C_{eff} vary: we deal with R_{top} variation here and C_{eff} variation in the next section.

In fact the variation of R_{top} with L is a rather trivial straight line relationship given by equation (2) with $Y = L$ and $R = R_{top}$. This is slightly obscured in Fig. 10 by using a logarithmic scale for L, but a linear scale for R_{top}. That has been done to show that for these data even though L varies by up to three orders of magnitude within the figure, the value of R_{top} itself only varies by at most an order of magnitude or so. Note also that the curves with higher m_* within Fig. 10 terminate at lower L values than the curves with lower m_* do. This is because (for nonzero m_* at least, for which there is no formal lower bound on ϕ_{top}) we have elected to terminate all curves at the same value of ϕ_{top}, specifically at $\phi_{top} = 0.0005$: this value was chosen arbitrarily but is considered to be in the regime of a very dry foam. Curves with higher m_* reach a given ϕ_{top} at a lesser L, and that then limits how much R_{top} can grow.

4.4. Effective concentration

In Fig. 11 we show how effective concentration of surface actives C_{eff} (as given by equation (3)) varies with foam column height L. Data for various m_* values are shown.

The first observation is that the $m_* = 0$ case is qualitatively different from the cases with nonzero m_*. When $m_* = 0$, the value of C_{eff} saturates at an upper limit even when foam column height L becomes arbitrarily large. This follows from equation (3) remembering that R is now fixed at a value R_0. Since (see section 4.1) it is known (Grassia, 2023) that ϕ_{top} can fall no lower than $V_{air}/(4R^2)$, this limits how much equation (3) allows C_{eff} to grow.

When m_* is nonzero however, the value of ϕ_{top} can fall much lower than this, and so C_{eff} can become very large indeed. This follows because, as already alluded to, there is a synergy between increasing foam

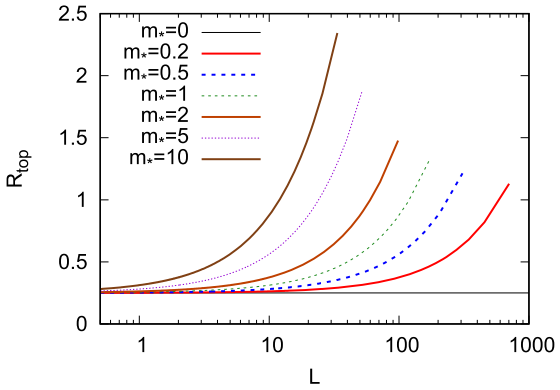

Fig. 10. Bubble size at the top R_{top} as a function of foam column height L. Note the logarithmic scale for L here, but the linear scale for R_{top}.

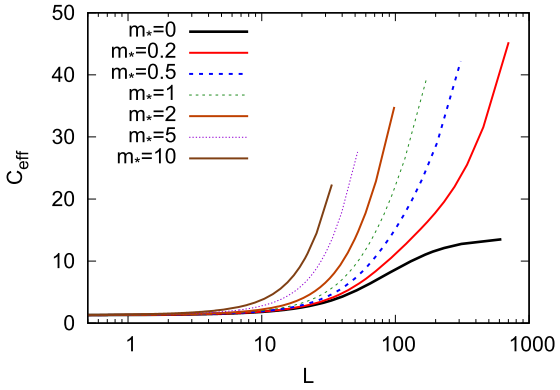

Fig. 11. Effective concentration C_{eff} versus foam column height L for various m_*.

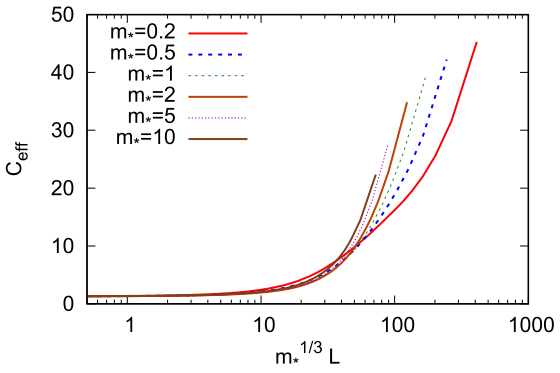

Fig. 12. Values of C_{eff} versus $m_*^{1/3}L$ for various m_*.

column height and increasing bubble size. This synergy leads to very dry foams (i.e. very low ϕ_{top}) which according to equation (3) are highly enriched.

As already mentioned, we have chosen here to terminate the curves for nonzero m_* when $\phi_{\text{top}} = 0.0005$ in each case. According to equation (3) this then means we terminate at a C_{eff} that scales inversely with R_{top}. Since the cases with larger m_* terminate at larger R_{top} (see Fig. 10), this implies that C_{eff} terminates at a slightly *lower* value as m_* increases. Of course this lower terminating value for C_{eff} is associated with a much smaller L, i.e. a greatly reduced foam column height. If we compare instead C_{eff} on the various curves in Fig. 11 at a fixed L (rather than at a fixed ϕ_{top}), it is then clear that the larger m_* case leads to higher effective concentration.

Just as we did with Fig. 8 (which collapsed together different ϕ_{top} curves) it is possible to collapse different C_{eff} curves together by rescaling the L axis. In Fig. 12 we rescale the axis as $m_*^{1/3}L$, which collapses together data reasonably well, at least for large m_*. As was the case for Fig. 8 the collapse is less good when m_* is small. Reasons why collapse is expected here when m_* is large, and why it involves $m_*^{1/3}L$ (and not $m_*^{1/2}L$ as in Fig. 8) are explained in section S6.

5. Conclusions

In the context of foam fractionation, we have analysed a simple model for transport of liquid through a foam column. The model predicts the amount of enrichment of a surface active material that thereby results. Within the model, the liquid flux through the foam column is itself spatially uniform, but spatial variations in bubble size are admitted. A parameter m_* was used to quantify this bubble size variation. In effect m_* measures the relative change in bubble size from bottom to top in a foam column of typical height.

A qualitative difference was found between systems with no bubble size variation whatsoever (m_* identically zero) and systems with slow spatial variation in bubble size (m_* small but finite). In the former case there was finite minimum liquid flux that the system could deliver and still meet the boundary condition at the top (no slip between liquid and air). This minimum liquid flux was simultaneously the *maximum* (the so called peak flux Q_{peak}) that could be delivered by air convection and gravity drainage alone without the aid of capillary suction. For small but finite m_* on the other hand, there was no formal minimum flux that could be delivered, and related with this, no limit upon how dry the foam could become at the top. The aforementioned peak flux Q_{peak} now in effect decreased moving upwards through the foam column and so, for a tall enough foam column, even a very small imposed liquid flux would eventually exceed Q_{peak}. A very dry foam leading to a highly enriched foamate could then result although foam column heights needed to scale proportionally to m_*^{-1} to achieve that.

Turning towards much larger m_* values, good enrichment of surface actives could be achieved even with comparatively short foam columns. Over much of the foam column, an approximate equilibrium between gravity drainage and capillary suction was found to occur, although the approximation could be improved by incorporating air convection effects. In the limit of large m_*, the liquid volume fraction at the top ϕ_{top} was shown to be a rapidly decreasing function of foam column height L. Having small ϕ_{top} (i.e. very dry foam) then ensured greatly enriched foamate. Equivalently the foam column height needed to attain a particular ϕ_{top} scaled like $m_*^{-1/2}$ in the large m_* limit. The foam column height needed to attain a given level of enrichment (measured here via an effective concentration C_{eff} of surface actives) scaled meanwhile like $m_*^{-1/3}$.

Overall we identified a synergy between increasing foam height (which even on its own dries out the foam) and increased bubble size at those increased heights (which then leads to much drier foams). Exploiting this synergy is likely to be useful in design and operation of foam fractionation systems, remembering that the drier the foam, the more enriched in surface actives the foamate becomes. It is expected to be particularly relevant in fractionation of comparatively dilute systems for which bubble size might well increase quite significantly moving up through the foam column.

As well as reflecting upon what has been achieved here, it is also worth highlighting what has not been considered. The present work has looked at just instantaneous behaviour of a fractionation column, but previous work demonstrated that fractionation performance evolves over time as the amounts of liquid in a fractionation column falls, and the height of the foam in the column grows to compensate (Grassia, 2023). In view of that, the synergy identified here between increasing foam column height and increasing bubble size is likely to become more significant over time.

Another important point, is that this study has been modelling based: the models still need to be checked against experiment. In particular the models used here for the assumed adsorption behaviour of surface actives have been greatly simplified compared to adsorption behaviour of complex molecules like proteins (Keshavarzi et al., 2022b). In respect of that, it is worth reflecting that the models herein make predictions both of liquid fractions and surface active concentrations/enrichments. Measurement of liquid fractions (typically involving determination of volumes and masses) are arguably easier to achieve than measurement of surface active concentrations (which might involve determination of surface tensions). That said, the models for liquid transport used here are not tied to a particular type of surface active: they could be applied e.g. to a protein (often targeted in flotation applications) but equally they could apply to a simple surfactant. To test the model it may be easier in the first instance to carry out experiments with a simple surfactant, and make measurements of liquid fractions. Once those aspects have been tested experimentally, it should then be possible to progress on to different types of surface actives, including measurements of concentrations/enrichment.

CRediT authorship contribution statement

P. G.: Funding acquisition; Conceptualization; Methodology; Investigation; Formal analysis; Visualization; Writing: Original Draft; Writing: Review and Editing. C. T.-U.: Formal analysis; Writing: Review and Editing.

Declaration of competing interest

The authors declare that they have no known competing financial interests or personal relationships that could have appeared to influence the work reported in this paper.

Data availability

Data presented here can be obtained from simple numerical integration of governing equations using parameter values that are provided in the text. Data files are provided with the supplementary material. Data analysed in this work can also be obtained from https://doi.org/10.15129/431c4ad8-bcf1-42ec-8fca-e62949b97b76.

Acknowledgements

The authors acknowledge support from EPSRC grant EP/V002937/1. C. T.-U. also acknowledges support from Centro de Investigación, Innovación y Creación UCT (CIIC-UCT).

Appendix A. Supplementary material

Supplementary material related to this article can be found online at https://doi.org/10.1016/j.ces.2023.119163.

References

Backleh-Sohrt, M., Ekici, P., Leupold, G., Parlar, H., 2005. Efficiency of foam fractionation for the enrichment of nonpolar compounds from aqueous extracts of plant materials. J. Nat. Prod. 68, 1386–1389. https://doi.org/10.1021/np049743e.

Brito-Parada, P.R., Neethling, S.J., Cilliers, J.J., 2013. Modelling the behaviour of the wetting front in non-standard forced foam drainage scenarios. Colloids Surf. A, Physicochem. Eng. Asp. 438, 21–27. https://doi.org/10.1016/j.colsurfa.2013.02.013.

Brown, L., Narsimhan, G., Wankat, P.C., 1990. Foam fractionation of globular proteins. Biotechnol. Bioeng. 36, 947–959. https://doi.org/10.1002/bit.260360910.

Buckley, T., Xu, X., Rudolph, V., Firouzi, M., Shukla, P., 2022. Review of foam fractionation as a water treatment technology. Sep. Sci. Technol. 57, 929–958. https://doi.org/10.1080/01496395.2021.1946698.

Burghoff, B., 2012. Foam fractionation applications. J. Biotechnol. 161, 126–137. https://doi.org/10.1016/j.jbiotec.2012.03.008.

Cantat, I., Cohen-Addad, S., Elias, F., Graner, F., Höhler, R., Pitois, O., Rouyer, F., Saint-Jalmes, A., 2013. Foams: Structure and Dynamics. Oxford University Press, Oxford.

Cox, S.J., Weaire, D., Hutzler, S., Murphy, J., Phelan, R., Verbist, G., 2000. Applications and generalizations of the foam drainage equation. Proc. R. Soc. Lond. Ser. A 456, 2441–2464. https://doi.org/10.1098/rspa.2000.0620.

Crofcheck, C., Loiselle, M., Weekley, J., Maiti, I., Pattanaik, S., Bummer, P.M., Jay, M., 2003. Histidine tagged protein recovery from tobacco extract by foam fractionation. Biotechnol. Prog. 19, 680–682. https://doi.org/10.1021/bp025738u.

de Lucena, S.L., Alves Miranda, E., Costapinto Santana, C., 1996. The effect of external reflux on the foam fractionation of proteins. Appl. Biochem. Biotechnol. 57, 57–65. https://doi.org/10.1007/BF02941688.

Díaz De Rienzo, M.A., Kamalanathan, I.D., Martin, P.J., 2016. Comparative study of the production of rhamnolipid biosurfactants by B-thailandensis E264 and P-aeruginosa ATCC 9027 using foam fractionation. Process Biochem. 51, 820–827. https://doi.org/10.1016/j.procbio.2016.04.007.

Du, L., Loha, V., Tanner, R.D., 2000. Modeling a protein foam fractionation process. Appl. Biochem. Biotechnol. 84, 1087–1099. https://doi.org/10.1385/abab:84-86:1-9:1087.

Du, L., Prokop, A., Tanner, R.D., 2002. Effect of bubble size on foam fractionation of ovalbumin. Appl. Biochem. Biotechnol. 98, 1075–1091. https://doi.org/10.1385/abab:98-100:1-9:1075.

Fainerman, V.B., Lucassen-Reynders, E.H., Miller, R., 2003. Description of the adsorption behaviour of proteins at water/fluid interfaces in the framework of a two-dimensional solution model. Adv. Colloid Interface Sci. 106, 237–259. https://doi.org/10.1016/S0001-8686(03)00112-X.

Fitch, B., 1966. Current theory and thickener design. Ind. Eng. Chem. 58, 18–28. https://doi.org/10.1021/ie50682a006.

Gerken, B., Nicolai, A., Linke, D., Zorn, H., Berger, R., Parlar, H., 2006. Effective enrichment and recovery of laccase C using continuous foam fractionation. Sep. Purif. Technol. 49, 291–294. https://doi.org/10.1016/j.seppur.2005.09.015.

Gochev, G., Retzlaff, I., Aksenenko, E.V., Fainerman, V.B., Miller, R., 2013. Adsorption isotherm and equation of state for β-lactoglobulin layers at the air/water surface. Colloids Surf. A, Physicochem. Eng. Asp. 422, 33–38. https://doi.org/10.1016/j.colsurfa.2013.01.008.

Grassia, P., 2023. Quasistatic model for foam fractionation. Chem. Eng. Sci. 275, 118721. https://doi.org/10.1016/j.ces.2023.118721.

Grassia, P., Cilliers, J.J., Neethling, S.J., Ventura-Medina, E., 2001. Quasi-one-dimensional foam drainage. Eur. Phys. J. E 6, 325–348. https://doi.org/10.1007/s10189-001-8047-3.

Grassia, P., Neethling, S.J., Cervantes, C., Lee, H.T., 2006. The growth, drainage and bursting of foams. Colloids Surf. A, Physicochem. Eng. Asp. 274, 110–124. https://doi.org/10.1016/j.colsurfa.2005.08.040.

Hilgenfeldt, S., Koehler, S.A., Stone, H.A., 2001. Dynamics of coarsening foams: accelerated and self-limiting drainage. Phys. Rev. Lett. 86, 4704–4707. https://doi.org/10.1103/PhysRevLett.86.4704.

Höhler, R., Seknagi, J., Kraynik, A., 2021. Capillary pressure, osmotic pressure and bubble contact areas in foams. Soft Matter 17, 6995–7003. https://doi.org/10.1039/D1SM00823D.

Hutzler, S., Tobin, S.T., Meagher, A.J., Marguerite, A., Weaire, D., 2013. A model system for foam fractionation. Proc. R. Soc. Lond. Ser. A 469, 20120727. https://doi.org/10.1098/rspa.2012.0727.

Keshavarzi, B., Krause, T., Schwarzenberger, K., Eckert, K., Ansorge-Schumacher, M.B., Heitkam, S., 2022a. Wash water addition on protein foam for removal of soluble impurities in foam fractionation process. Colloids Surf. A, Physicochem. Eng. Asp. 655, 130215. https://doi.org/10.1016/j.colsurfa.2022.130215.

Keshavarzi, B., Krause, T., Sikandar, S., Schwarzenberger, K., Eckert, K., Ansorge-Schumacher, M.B., Heitkam, S., 2022b. Protein enrichment by foam fractionation: experiment and modeling. Chem. Eng. Sci. 256, 117715. https://doi.org/10.1016/j.ces.2022.117715.

King, C.J., 1980. Separation Processes, 2nd edition. McGraw-Hill Chemical Engineering Series. McGraw-Hill, New York.

Koehler, S.A., Hilgenfeldt, S., Stone, H.A., 1999. Liquid flow through aqueous foams: the node-dominated foam drainage equation. Phys. Rev. Lett. 82, 4232–4235. https://doi.org/10.1103/PhysRevLett.82.4232.

Koehler, S.A., Hilgenfeldt, S., Stone, H.A., 2000. A generalized view of foam drainage: experiment and theory. Langmuir 16, 6327–6341. https://doi.org/10.1021/la9913147.

Kou, Q., Li, J., Zhao, B., Wu, Z., 2015. Recovery of streptomycin sulfate from the wastewater using foam fractionation coupled with adsorption separation for reusing sodium dodecyl sulfate. J. Chem. Technol. Biotechnol. 90, 874–879. https://doi.org/10.1002/jctb.4388.

Lemlich, R., 1968. Principles of foam fractionation. In: Perry, E.S. (Ed.), Progress in Separation and Purification. Interscience, New York, pp. 1–56.

Lemlich, R. (Ed.), 1972. Adsorptive Bubble Separation Techniques. Academic Press Inc., New York, London.

Li, N., Li, W., Wu, Z., Xu, Y., Shu, T., Lu, K., Zhao, Y., 2018. Recovery of silk sericin from the filature wastewater by using a novel foam fractionation column. Chem. Eng. Process., Process Intensific. 129, 37–42. https://doi.org/10.1016/j.cep.2018.04.027.

Li, R., Fu, N., Wu, Z., Wang, Y., Liu, W., Wang, Y., 2016. Enhancing protein self-association at the gas–liquid interface for foam fractionation of bovine serum albumin from its highly diluted solution. Chem. Eng. Res. Des. 109, 638–646. https://doi.org/10.1016/j.cherd.2016.03.018.

Linke, D., Zorn, H., Gerken, B., Parlar, H., Berger, R.G., 2007. Laccase isolation by foam fractionation: new prospects of an old process. Enzyme Microb. Technol. 40, 273–277. https://doi.org/10.1016/j.enzmictec.2006.04.010.

Liu, W., Zhang, M., Lv, Y., Tian, S., Li, N., Wu, Z., 2017. Foam fractionation for recovering whey soy protein from whey wastewater: strengthening foam drainage using a novel internal component with superhydrophobic surface. J. Taiwan Inst. Chem. Eng. 78, 39–44. https://doi.org/10.1016/j.jtice.2017.05.027.

Lockwood, C.E., Bummer, P.M., Jay, M., 1997. Purification of proteins using foam fractionation. Pharm. Res. 14, 1511–1515. https://doi.org/10.1023/a:1012109830424.

Lorenceau, E., Louvet, N., Rouyer, F., Pitois, O., 2009. Permeability of aqueous foams. Eur. Phys. J. E 28, 293–304. https://doi.org/10.1140/epje/i2008-10411-7.

Martin, P.J., Dutton, H.M., Winterburn, J.B., Baker, S., Russell, A.B., 2010. Foam fractionation with reflux. Chem. Eng. Sci. 65, 3825–3835. https://doi.org/10.1016/j.ces.2010.03.025.

Mathews, A., Bishnoi, P.R., Svrcek, W.Y., 1979. Treatment of oil contaminated waste waters by foam fractionation. Water Res. 13, 385–391. https://doi.org/10.1016/0043-1354(79)90028-9.

Miller, R., Fainerman, V.B., Leser, M.E., Michel, M., 2004. Kinetics of adsorption of proteins and surfactants. Curr. Opin. Colloid Interface Sci. 9, 350–356. https://doi.org/10.1016/j.cocis.2004.08.002.

Mukhopadhyay, G., Khanam, J., Nanda, A., 2010. Protein removal from whey waste by foam fractionation in a batch process. Sep. Sci. Technol. 45, 1331–1339. https://doi.org/10.1080/01496391003697382.

Neethling, S.J., Brito-Parada, P.R., 2018. Predicting flotation behaviour: the interaction between froth stability and performance. Miner. Eng. 120, 60–65. https://doi.org/10.1016/j.mineng.2018.02.002.

Neethling, S.J., Cilliers, J.J., Woodburn, E.T., 2000. Prediction of the water distribution in a flowing foam. Chem. Eng. Sci. 55, 4021–4028. https://doi.org/10.1016/S0009-2509(00)00054-3.

Neethling, S.J., Lee, H.T., Grassia, P., 2005. The growth, drainage and breakdown of foams. Colloids Surf. A, Physicochem. Eng. Asp. 263, 184–196. https://doi.org/10.1016/j.colsurfa.2004.12.014.

Pitois, O., Lorenceau, E., Louvet, N., Rouyer, F., 2009. Specific surface area model for foam permeability. Langmuir 25, 97–100. https://doi.org/10.1021/la8029616.

Rajabi, H., Grassia, P., 2023. Transport of soluble surfactant on and within a foam film in the context of a foam fractionation process. Chem. Eng. Sci. 265, 118171. https://doi.org/10.1016/j.ces.2022.118171.

Saleh, Z.S., Hossain, M.M., 2001. A study of the separation of proteins from multicomponent mixtures by a semi-batch foaming process. Chem. Eng. Process., Process Intensific. 40, 371–378. https://doi.org/10.1016/S0255-2701(01)00115-5.

Sarhan, A.R., Naser, J., Brooks, G., 2017a. CFD modeling of three-phase flotation column incorporating a population balance model. Proc. Eng., Adv. Mater. Process.Technol. Conf. 184, 313–317. https://doi.org/10.1016/j.proeng.2017.04.100.

Sarhan, A.R., Naser, J., Brooks, G., 2017b. Numerical simulation of froth formation in aerated slurry coupled with population balance modelling. Can. Metall. Q. 56, 45–57. https://doi.org/10.1080/00084433.2016.1268771.

Sarhan, A.R., Naser, J., Brooks, G., 2018a. CFD model simulation of bubble surface area flux in flotation column reactor in presence of minerals. Int. J. Mining Sci. Technol. 28. https://doi.org/10.1016/j.ijmst.2018.05.004.

Sarhan, A.R., Naser, J., Brooks, G., 2018b. CFD modeling of bubble column: influence of physico-chemical properties of the gas/liquid phases properties on bubble formation. Sep. Purif. Technol. 201, 130–138. https://doi.org/10.1016/j.seppur.2018.02.037.

Shea, A.P., Crofcheck, C.L., Payne, F.A., Xiong, Y.L., 2009. Foam fractionation of α-lactalbumin and β-lactoglobulin from a whey solution. Asia-Pac. J. Chem. Eng. 4, 191–203. https://doi.org/10.1002/apj.221.

Stevenson, P., 2012. Foam Engineering: Fundamentals and Applications. John Wiley and Sons, Chichester, UK.

Stevenson, P., 2014. Foam Fractionation: Principles and Process Design. Taylor and Francis, Boca Raton FL.

Stevenson, P., Jameson, G.J., 2007. Modelling continuous foam fractionation with reflux. Chem. Eng. Process., Process Intensific. 46, 1286–1291. https://doi.org/10.1016/j.cep.2006.10.010.

Tian, S., Wu, Z., Liu, W., Zhang, M., Lv, Y., Xu, Y., Liu, G., Zhao, Y., 2018. Effective recovery of casein from its highly diluted solution by using a technology of foam fractionation coupled with isoelectric precipitation. J. Food Eng. 216, 72–80. https://doi.org/10.1016/j.jfoodeng.2017.07.004.

Tobin, S.T., Weaire, D., Hutzler, S., 2014. Theoretical analysis of the performance of a foam fractionation column. Proc. R. Soc. Lond. Ser. A 470, 20130625. https://doi.org/10.1098/rspa.2013.0625.

Tong, M., Cole, K., Neethling, S.J., 2011. Drainage and stability of 2D foams: foam behaviour in vertical Hele-Shaw cells. Colloids Surf. A, Physicochem. Eng. Asp. 382, 42–49. https://doi.org/10.1016/j.colsurfa.2010.11.007.

Usher, S.P., Scales, P.J., 2005. Steady state thickener modelling from the compressive yield stress and hindered settling function. Chem. Eng. J. 111, 253–261. https://doi.org/10.1016/j.cej.2005.02.015.

Verbist, G., Weaire, D., Kraynik, A.M., 1996. The foam drainage equation. J. Phys. Condens. Matter 8, 3715–3731. https://doi.org/10.1088/0953-8984/8/21/002.

Vitasari, D., Grassia, P., Martin, P.J., 2013. Surfactant transport onto a foam lamella. Chem. Eng. Sci. 102, 405–423. https://doi.org/10.1016/j.ces.2013.08.041.

Weaire, D., Hutzler, S., 1999. The Physics of Foams. Oxford University Press, Oxford.

Weaire, D., Hutzler, S., Verbist, G., Peters, E., 1997. A review of foam drainage. Adv. Chem. Phys. 102, 315–374. https://doi.org/10.1002/9780470141618.ch5.

Wu, Z., Shu, T., Zhang, M., Liu, W., 2020a. Foam fractionation for effective recovery of leaf protein from alfalfa (Medicago sativa L). Sep. Sci. Technol. 55, 1388–1397. https://doi.org/10.1080/01496395.2019.1586725.

Wu, Z., Yin, H., Liu, W., Huang, D., Hu, N., Yang, C., Zhao, X., 2020b. Xanthan gum assisted foam fractionation for the recovery of casein from the dairy wastewater. Prepar. Biochem. Biotechnol. 50, 37–46. https://doi.org/10.1080/10826068.2019.1658119.

Yeo, L.Y., Matar, O.K., Perez de Ortiz, E.S., Hewitt, G.F., 2001. The dynamics of Marangoni-driven local film drainage between two drops. J. Colloid Interface Sci. 241, 233–247. https://doi.org/10.1006/jcis.2001.7743.